GENERATING A PERSPECTIVE IMAGE FROM A PANORAMIC IMAGE BY THE SWUNG-TO-CYLINDER PROJECTION

Che-Han Chang[†] *Wei-Sheng Lai*[‡] *Yung-Yu Chuang*[⋆]

[†]HTC [‡]UC Merced [⋆]National Taiwan University

ABSTRACT

This paper proposes a swung-to-cylinder projection model for mapping a sphere to a plane. It can be used to create a semi-perspective image from a panoramic image. The model has two steps. In the first step, the sphere is projected onto a swung surface constructed by a circular profile and a rounded rectangular trajectory. In the second step, the projected image on the swung surface is mapped onto a cylinder through the perspective projection. We also propose methods for automatically determining proper parameters for the projection model based on image content. The proposed model is simple, efficient and easy to control. Experiments and analysis demonstrate its effectiveness.

***Index Terms*—** Projection models, swung surfaces.

1. INTRODUCTION

Capturing a scene with a wide field of view from a single viewpoint records rich visual information of the scene. Responding to the need of taking images with wider fields of view, there are more and more wide-angle cameras available on the market, such as GoPro and Ricoh Theta. The recorded information can be defined with a viewing sphere which stores the incident radiance at the viewpoint from any incoming direction. For viewing wide-angle images defined on a viewing sphere, it is often required to map from the viewing sphere to an image plane. However, it is impossible to map from a sphere to a plane without introducing distortions. Thus, projection models have to trade off different types of distortions and none can avoid all distortions.

For striking a good compromise among distortions, Chang et al. proposed the swung-to-plane projection model [1]. It consists of two steps. The first step projects the viewing sphere onto a swung surface which is constructed by circling a circular profile around a rounded rectangular trajectory. The second step maps the projection on the swung surface onto the image plane through the perspective projection. Although generating better perspective images from wide-angle images than previous models, the swung-to-plane

This work was supported by MOST under grants 104-2628-E-002-003-MY3 and 107-2634-F-002-007.

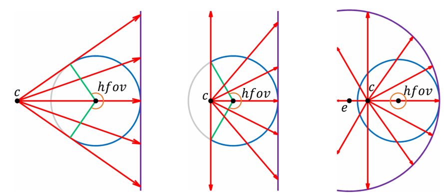

(a) (b) (c)

Fig. 1. Horizontal FOV analysis. We show the maximal hFOV on the xz plane. (a) Projection to the projection plane (the purple line) with $d > 1$ (b) Projection to the projection plane with $0 < d < 1$ (c) Projection to a projection cylinder (the purple curve).

projection model has a limited hFOV and suffers from serious distortion when viewing with a larger hFOV. Fig. 1 (a)(b) illustrates the maximal hFOV when projecting from a unit sphere/cylinder/swung surface to a projection plane. The maximal hFOV reachs $360°$ when $d = 1$ (d is the distance between the center of the viewing sphere and the center of the perspective projection at the second step), but it would require infinite space. In order to show a scene with the $360°$ hFOV within finite space, we replace the projection plane in the second step with a *projection cylinder* (Fig. 1 (c)). The resultant image is obtained by flattening the projection cylinder. We call it the swung-to-cylinder model. The swung-to-plane projection can be taken as a special case of the proposed swung-to-cylinder projection model. The swung-to-cylinder model is advantageous for viewing panoramas with the $360°$ hFOV and a large vFOV. We also present methods for automatically optimizing parameters of the projection models based on image content. We demonstrate that our model gives more pleasant views for wide-angle and panoramic images.

2. RELATED WORK

For wide-angle images, Zorin and Barr [2] proposed a one-parameter family of projections that interpolate between the rectilinear and stereographic projections. Ying and Hu [3] proposed a unified imaging model for central catadioptric and fisheye cameras. Sharpless et al. [4] proposed the Pannini projection for viewing wide-angle perspective images. Some approaches require user assistance for viewing panoramas and wide-angle images [5, 6, 7].

For panoramic projections, cylindrical projections [8] are widely used because of their simplicity and wide hFOV which meets the need of panoramas. Zelnik-Manor et al. [9] proposed a multi-plane projection as an alternative to the cylindrical projection. Kopf et al. [10] presented an interactive viewer for gigapixel panoramas. Our projection model is able to render the 360° hFOV for panoramas, and reduce the amount of distortion by automatically optimizing parameters.

He et al. [11] proposed a content-aware warping algorithm that warps the irregular boundary of panoramas to be rectangular. They further extended this method to preserve "geodesic" lines [12]. Both Carroll et al.'s [5] and He et al.'s [11] methods are content-aware local warping, while our method is a global projection with few parameters that could be estimated from the image content. There exist researches on creating panoramas from different viewpoints. Agarwala et al. [13] proposed a system for creating multi-viewpoint panoramas of street scenes from fisheye videos. Kopf et al. [14] presented a system for browsing multi-perspective street views. Different from them, our projection model is designed for generating an as-perspective-as-possible image from a single viewpoint.

3. THE PROJECTION MODEL

3.1. The swung-to-cylinder projection model

The proposed swung-to-cylinder projection model maps from a viewing sphere to the projection cylinder as illustrated in Fig. 2. Given a point p on the sphere (the orange surface), the first step projects p onto a point $\bar{p}$ on a swung surface S (the blue surface) through a line emanating from the center of the sphere. This step is exactly the same as the first step in the swung-to-plane projection [1]. By construction, the 3D Euclidean coordinate $\bar{\mathbf{x}}_p$ of point $\bar{p}$ is $(\bar{x}_p, \bar{y}_p, \bar{z}_p) = (\bar{r}_p \sin\phi_p \cos\theta_p, \bar{r}_p \sin\phi_p \sin\theta_p, \bar{r}_p \cos\phi_p)$.

In the second step, $\bar{p}$ on the swung surface S is projected onto a point $\hat{p}$ on the projection cylinder (the purple surface) through a line emanating from the center of projection c. As shown in Fig. 2(b), c is set to lie on the negative z axis with coordinate $\mathbf{x}_c = (0, 0, -d)$. The projection cylinder has a radius R and is centered at the point e with the coordinate $\mathbf{x}_e = (0, 0, 1-R)$. The projection cylinder intersects with the surface S at the point $(0, 0, 1)$. We characterize the projection cylinder by its curvature $\kappa = 1/R$. The point $\hat{p}$ is the intersection between the projection cylinder and a line formed by c and $\bar{p}$ (the red line shown in Fig. 2(b)). By expressing $\hat{p}$ as a point on the cylinder and as a point on the line respectively, we have the following equations

$$\hat{\mathbf{x}}_p = \mathbf{x}_c + \alpha_p(\bar{\mathbf{x}}_p - \mathbf{x}_c), \tag{1}$$

$$\hat{\mathbf{x}}_p = \mathbf{x}_e + [R\sin\beta_p, h_p, R\cos\beta_p]^T, \tag{2}$$

where $\hat{\mathbf{x}}_p$ is the Euclidean coordinate of $\hat{p}$; α_p is the parameter on the line; (β_p, h_p) is the coordinate on the projection cylinder. $\hat{\mathbf{x}}_p$ can be derived by solving Equation (1) and (2). The formulae of α_p, β_p and h_p are as follows

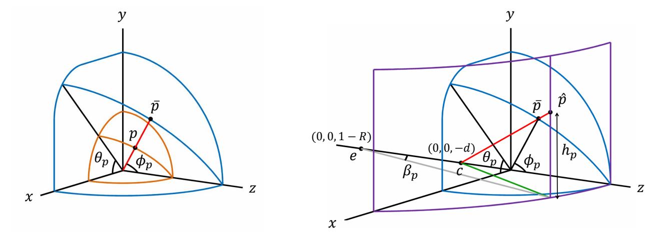

(a) The first step (b) The second step

Fig. 2. The two steps in the swung-to-cylinder model.

$$\alpha_p = \frac{-b_p t + \sqrt{\bar{x}_p^2(R^2 - t^2) + b_p^2 R^2}}{\bar{x}_p^2 + b_p^2}, \tag{3}$$

$$\beta_p = \tan^{-1}\left(\frac{\alpha_p \bar{x}_p}{\alpha_p b_p + t}\right), \tag{4}$$

$$h_p = \alpha_p \bar{y}_p, \tag{5}$$

where $b_p = \bar{z}_p + d$ and $t = R - d - 1$. The formula of $\hat{\mathbf{x}}_p$ can be obtained by substituting Equation (3) into Equation (1). After projections, the projection cylinder is flattened as the image plane. Thus, the 3D coordinate of $\hat{p}$ is mapped to a 2D coordinate (u_p, v_p) on the image plane. Based on the formula in Equation (2), the 2D coordinate of $\hat{p}$ can be written as

$$(u_p, v_p) = (R\beta_p, h_p). \tag{6}$$

To sum up, with Equation (3), (4), (5) and (6), one can relate the 3D spherical coordinate $(1, \theta_p, \phi_p)$ of a point p on the viewing sphere with the 2D coordinate (u_p, v_p) of its projection on the image plane.

3.2. Comparisons with previous models

There are several parameters in the swung-to-cylinder projection model: d, κ and $R(\theta)$, which are respectively the center of projection in the second step, the curvature of the projection cylinder and the trajectory curve of the swung surface. When the rounded rectangle is chosen as the trajectory curve, $R(\theta)$ is represented by two parameters, l and h, the roundness and the aspect ratio of the rounded rectangle. By setting $\kappa = 0$, the swung-to-cylinder projection model reduces to the swung-to-plane projection model. The swung-to-cylinder projection model further unifies the following models: the cylindrical projection, Kopf's one-parameter family of projections [10], and the Pannini projections [4] as summarized in Table 1.

We analyze the distortions of the central cylindrical projection, the stereographic Pannini projection, Kopf et al.'s model and our swung-to-cylinder projection using Tissot's indicatrix [15] as shown in the left column of Fig. 3. For the cylindrical projection, the shape and area distortions are aggravated as the vertical FOV increases. The stereographic

Table 1. Summary of different projection models. Our swung-to-cylinder projection model unifies these projections.

	d	κ	$R(\theta)$
Cylindrical	$[0, 1]$	1	$\sqrt{1 + \tan^2(\theta)}$
−Central Cylindrical	0	1	n/a
Kopf *et al*. [10]	0	$[0, 1]$	n/a
Pannini [4]	$[0, \infty]$	0	$\sqrt{1 + \tan^2(\theta)}$
− Stereographic Pannini	1	0	$\sqrt{1 + \tan^2(\theta)}$
Swung-to-plane model [1]	$[0, 1]$	0	rounded rectangle
Swung-to-cylinder model	$[0, 1]$	$[0, 1]$	rounded rectangle

Pannini projection drastically enlarges the two sides of the image. When comparing to Kopf et al.'s model, our swung-to-cylinder projection has advantages when viewing scenes with large vertical FOVs. We then compare these methods on line preserving using grid patterns shown in the middle column of Fig. 3. All models other than the swung-to-cylinder projection model keep vertical lines straight. Although the swung-to-cylinder projection model does not guarantee preserving all vertical lines, one could find a proper aspect ratio h to ensure all visible vertical lines are straight. For other lines, line bending is the worst in the cylindrical projection. The stereographic Pannini projection maintains the straightness of lines that pass through the image center at the price of severe area distortions. Kopf et al.'s model and the swung-to-cylinder projection model have similar effects on line preserving because both models allow the radius of projection cylinder to vary and achieve a good balance between distortion and line preserving. However, Kopf et al.'s model could cause serious shape distortion when viewing with a larger vertical FOV as shown in Fig. 4. Our projection looks more perspective than Kopf et al.'s model.

3.3. Parameter optimization

There are four parameters in our swung-to-cylinder projection model, d, κ, h and l. We provide users with an option for automatically setting parameters based on the image content. The content features are lines and image saliency. For image saliency, we use the gradient magnitude to indicate visual saliency on the viewing sphere. We construct a set of points $P = \{p_1, p_2, ..., p_n\}$ on the viewing sphere by regularly taking samples for the spherical coordinate (θ, ϕ). The saliency s_i of each sample point p_i is obtained by computing its gradient magnitude on the viewing sphere. For finding line structures, we use a cube map to project the viewing sphere onto six perspective views, and then use the LSD line segment detector [16] to find line segments. Each line segment corresponds to an arc l_j of a great circle on the viewing sphere.

Our energy function $E(d, \kappa)$ is composed of three terms respectively for shape distortions, area distortions and line distortions. We make use of Tissot's indicatrix for measuring shape distortions and area distortions. An infinitesimal circle at p_i on the viewing sphere is mapped to an ellipse ψ_i

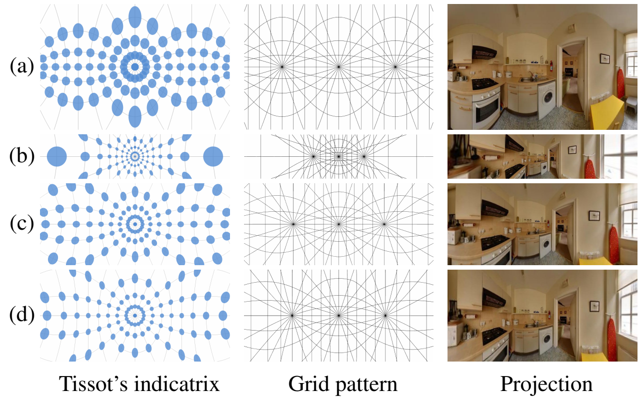

Fig. 3. Tissot's indicatrix and grid patterns. (a) Central cylindrical projection ($d = 0$, $\kappa = 1$), (b) Stereographic Pannini projection [4] ($d = 1$, $\kappa = 0$), (c) Kopf et al.'s model [10] ($d = 0$, $\kappa = 0.6$). (d) Our swung-to-cylinder projection ($d = 0.6$, $\kappa = 0.6$, $l = 0.75$, $h = 3$). The left column shows the Tissot's indicatrix. The grey lines are contours of either constant θ or constant ϕ. The middle column shows the projection of three sets of orthogonal scene lines. The right column shows the projection images.

on the image plane after the projection. We then use the semi-major axis and the semi-minor axis of the ellipse ψ_i to measure shape and area distortions.

For shape distortions, we would like to preserve the conformality of the projection. If p_i undergoes an conformal projection, then its ellipse ψ_i should be a circle. Therefore, we require that the aspect ratio of ψ_i is close to 1. Therefore, the shape distortion term is defined as

$$E_s(d, \kappa) = \sum_{p_i \in P'} s(p_i) \cdot \left(\frac{\lambda_1(p_i, d, \kappa)}{\lambda_2(p_i, d, \kappa)} - 1 \right)^2, \qquad (7)$$

where $P' \subset P$ is the set of sample points that are visible on the image plane; $\lambda_1(p_i, d, \kappa)$ and $\lambda_2(p_i, d, \kappa)$ return the semi-major axis and semi-minor axis of the ellipse ψ_i respectively; the saliency $s(p_i)$ is incorporated into the energy and serves as a weighting factor.

For area distortions, we would like to maintain the area of local regions after the projection. If a projection is area-preserving, we have $\lambda_1 \lambda_2 = 1$. The area distortion energy is then defined as

$$E_a(d, \kappa) = \textstyle\sum_{p_i \in P'} s(p_i) \cdot (\lambda_1(p_i, d, \kappa)\lambda_2(p_i, d, \kappa) - 1)^2. \quad (8)$$

For the line distortion term, we would to like to minimize the bending of lines. An arc l_j of a great circle on the viewing sphere is mapped to a curve on the image plane after the projection. We compute the tangent vectors of the curve at its two endpoints and denote them as $\mathbf{t}_1(j, d, \kappa)$ and $\mathbf{t}_2(j, d, \kappa)$. The line distortion term is then defined by measuring the an-

(a) Central cylindrical projection (b) Central cylindrical projection

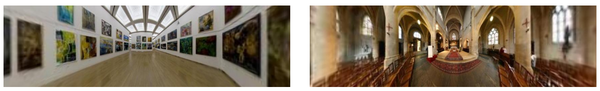

(c) Stereographic Pannini projection (d) Stereographic Pannini projection

(e) Kopf et al.'s model (f) Kopf et al.'s model

(g) Ours (h) Ours

Fig. 4. Comparisons of the central cylindrical projection, the stereographic Pannini projection, Kopf et al.'s model and our swung-to-cylinder projection model.

gle between them,

$$E_l(d,\kappa) = \sum_j \arccos\left(\frac{\mathbf{t}_1(j,d,\kappa)\cdot\mathbf{t}_2(j,d,\kappa)}{\|\mathbf{t}_1(j,d,\kappa)\|\,\|\mathbf{t}_2(j,d,\kappa)\|}\right). \quad (9)$$

The energy function is aggregated as a weighted sum of the above three energy terms

$$E(d,\kappa) = E_s(d,\kappa) + w_a E_a(d,\kappa) + w_l E_l(d,\kappa). \quad (10)$$

The energy is a nonlinear function in terms of d and κ. The optimization is performed by regularly sampling the 2D parameter space (d,κ), evaluating the energy for the sampled values and picking up the one with the lowest energy. We used $w_a = 0.01$ and $w_l = 60$ in our experiments. After determining d and κ, we find a good aspect ratio h with zero roundness, and then seek the best roundness of the rounded rectangle with that aspect ratio using a method similar to the one proposed by Chang et al. [1].

4. EXPERIMENTS

We implemented our methods on a PC with a 3.4GHz CPU and 4GB RAM. As for the running time, for an output image

(a)

(b)

(c)

(d)

(e)

Fig. 5. Full spherical panorama visualizations. (a) The cylindrical projection. (b) The Pannini projection. (c) The stereographic projection. (d) The swung-to-plane projection. (e) Our swung-to-cylinder projection.

with the 800×400 resolution, our implementation of the swung-to-cylinder model took around 5 minutes to find the parameters, and the projection took less than 1 second. We have compared our swung-to-cylinder projection models with previous models and discussed their strengths and weaknesses in Fig. 3. In Fig. 4, we show more results of comparing our model with previous models. For Kopf et al.'s model, we uniformly sample κ and select the best κ which minimizes the energy function in Equation (10). In general, our swung-to-cylinder projection model achieves a good balance between each distortion. It presents better perspective effects than the central cylindrical projection and Kopf et al.'s model while having much less distortion than the stereographic Pannini projection. Fig. 5 compares results when viewing full spherical panoramas with a 360° horizontal FOV.

5. CONCLUSION

This paper proposes a projection model for visualizing wide-angle images and panoramas with 360° hFOV. Our swung-to-cylinder projection model generalizes the swung-to-plane model by projecting from the swung surface to the projection cylinder in the second step. It performs better when viewing with a full horizontal FOV of 360°. The proposed model also unifies several previous models and strike a better balance between shape/area distortions and line preserving.

6. REFERENCES

[1] Che-Han Chang, Min-Chun Hu, Wen-Huang Cheng, and Yung-Yu Chuang, "Rectangling stereographic projection for wide-angle image visualization," in *Proceedings of IEEE International Conference on Computer Vision (ICCV 2013)*, December 2013, pp. 2824–2831.

[2] Denis Zorin and Alan H Barr, "Correction of geometric perceptual distortions in pictures," in *Proceedings of ACM SIGGRAPH*, 1995, pp. 257–264.

[3] Xianghua Ying and Zhanyi Hu, "Can we consider central catadioptric cameras and fisheye cameras within a unified imaging model," in *Proceedings of ECCV 2004*, 2004, pp. 442–455.

[4] Thomas K Sharpless, Bruno Postle, and Daniel M German, "Pannini: a new projection for rendering wide angle perspective images," in *Proceedings of the Sixth international conference on Computational Aesthetics in Graphics, Visualization and Imaging*, 2010, pp. 9–16.

[5] Robert Carroll, Maneesh Agrawal, and Aseem Agarwala, "Optimizing content-preserving projections for wide-angle images," in *ACM Transactions on Graphics*, 2009, vol. 28, p. 43.

[6] Jin Wei, Chen-Feng Li, Shi-Min Hu, Ralph R Martin, and Chiew-Lan Tai, "Fisheye video correction," *IEEE TVCG*, vol. 18, no. 10, pp. 1771–1783, 2012.

[7] Johannes Kopf, Dani Lischinski, Oliver Deussen, Daniel Cohen-Or, and Michael Cohen, "Locally adapted projections to reduce panorama distortions," in *Computer Graphics Forum*, 2009, vol. 28, pp. 1083–1089.

[8] John Parr Snyder, *Map projections–A working manual*, Number 1395. USGPO, 1987.

[9] Lihi Zelnik-Manor, Gabriele Peters, and Pietro Perona, "Squaring the circle in panoramas," in *Proceedings of ICCV 2005*, 2005, vol. 2, pp. 1292–1299.

[10] Johannes Kopf, Matt Uyttendaele, Oliver Deussen, and Michael F Cohen, "Capturing and viewing gigapixel images," *ACM Transactions on Graphics*, vol. 26, no. 3, pp. 93, 2007.

[11] Kaiming He, Huiwen Chang, and Jian Sun, "Rectangling panoramic images via warping," *ACM Transactions on Graphics (TOG)*, vol. 32, no. 4, pp. 79, 2013.

[12] Dongping Li, Kaiming He, Jian Sun, and Kun Zhou, "A geodesic-preserving method for image warping," in *Proceedings of the IEEE Conference on Computer Vision and Pattern Recognition*, 2015, pp. 213–221.

[13] Aseem Agarwala, Maneesh Agrawala, Michael Cohen, David Salesin, and Richard Szeliski, "Photographing long scenes with multi-viewpoint panoramas," in *ACM Transactions on Graphics*, 2006, vol. 25, pp. 853–861.

[14] Johannes Kopf, Billy Chen, Richard Szeliski, and Michael Cohen, "Street slide: browsing street level imagery," *ACM Transactions on Graphics*, vol. 29, no. 4, pp. 96, 2010.

[15] Piotr H Laskowski, "The traditional and modern look at tissot's indicatrix," *The American Cartographer*, vol. 16, no. 2, 1989.

[16] R Grompone Von Gioi, Jeremie Jakubowicz, J-M Morel, and Gregory Randall, "LSD: A fast line segment detector with a false detection control," *IEEE PAMI*, vol. 32, no. 4, pp. 722–732, 2010.